

## Enhancement of Terbium(III)-Centered Luminescence by Tuning the Triplet Energy Level of Substituted Pyridylamino-4-R-Phenoxy Tripodal Ligands

Jorge Manzur,\* Carolina Poblete, Jeannette Morales, Ricardo Costa de Santana,\* Lauro June Queiroz Maia, Andres Vega, Pablo Fuentealba, and Evgenia Spodine\*

Cite This: *Inorg. Chem.* 2020, 59, 5447–5455

Read Online

ACCESS |

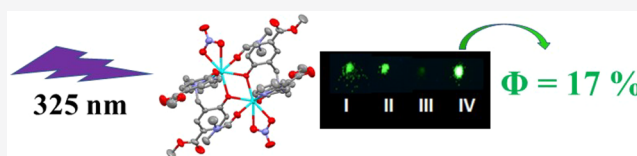
Metrics & More

Article Recommendations

Supporting Information

**ABSTRACT:** A series of luminescent phenoxy-bridged dinuclear Tb<sup>III</sup> complexes with tripodal ligands, 2,2'-[[2-(2-pyridinylmethyl)imino]di(methylene)]-bis(4-R-phenol), where R = CH<sub>3</sub> (L<sup>CH<sub>3</sub></sup>) (I), Cl (L<sup>Cl</sup>) (II), CH<sub>3</sub>O (L<sup>CH<sub>3</sub>O</sup>) (III), COOCH<sub>3</sub> (L<sup>COOCH<sub>3</sub></sup>) (IV), were prepared to probe the effect of *para*-substitution on the phenol ring of the ligand on the Tb<sup>III</sup> luminescence. For these Tb<sup>III</sup>

complexes a complete suppression of the ligand-centered fluorescence is observed, which demonstrates an efficient ligand-to-metal energy transfer. Complex IV was found to be the one that shows the greater intensity of the emission at room temperature. The obtained quantum yields follow the trend IV > II ≫ I > III. The quantum yield for II and IV is approximately five times greater than those obtained for I and III, indicating that the L<sup>Cl</sup> and L<sup>COOCH<sub>3</sub></sup> are better sensitizers of the Tb<sup>III</sup> ions. These results were rationalized in terms of the variation of the energy gap between the triplet level (T<sub>1</sub>) of the ligand and the emissive <sup>5</sup>D<sub>4</sub> level of Tb<sup>III</sup>, due to the electron-acceptor or electron-donor properties of the substituents. The τ<sub>av</sub> values are in the millisecond range for all the studied complexes and resulted independent of temperature. The Commission International d'Éclairage coordinates (CIE) for all complexes are in the green color region, being insensitive to the variation of temperature. Moreover, the color purity (CP) is ca. 90% for all complexes, being ca. 100% for IV. Thus, the introduction of electron-acceptor substituents on the ligand permitted us to improve the luminescent properties of the Tb<sup>III</sup> complexes.



### INTRODUCTION

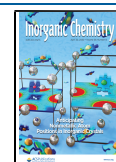
Trivalent rare-earth ions remain widely used due to their narrow emission, arising from the intraconfigurational  $4f^n - 4f^n$  transitions and long emission decay times (up to milliseconds).<sup>1–5</sup> However, lanthanide(III) ions have low absorption coefficients in the UV–visible spectrum,<sup>3</sup> since the absorption are Laporte forbidden, resulting in weak emission. So, an efficient way to avoid this problem lies in the use of organic ligands coupled to lanthanide(III) ions, producing the so-called “antenna effect”.<sup>6</sup> For an efficient energy transfer, the excited state of the ligand (T<sub>1</sub>) should be slightly higher in energy than the lowest excited state of the lanthanide, permitting a proper match between both states. The importance of the energy gap between the triplet state of the ligand and the emissive state of the lanthanide ion was remarked by Parker et al.<sup>7</sup> These authors examined, in aqueous solution, the emission of Eu<sup>III</sup>, Gd<sup>III</sup>, and Tb<sup>III</sup> complexes with octadentate macrocyclic ligands, 1,4,7,10-tetraazacyclododecane, together with the phosphinate analogues, and studied the efficiency of the energy-transfer process.<sup>7</sup> Shiraiishi et al. also studied the photophysical properties in water of Eu<sup>III</sup> and Tb<sup>III</sup> complexes with the same macrocyclic ligands and reported the influence of the coordinated water molecules on the emission of the lanthanide complexes.<sup>8</sup> Calculations done on Eu<sup>III</sup> and Gd<sup>III</sup> tris bipyridine cryptate complexes also permitted to assess

a detrimental effect of coordinated water molecules on the emission of these lanthanide(III) ions.<sup>9</sup> Moreover, Chauvin et al. analyzed the effect of both the energy gap between the triplet state of the ligand and the emissive state of the lanthanide ion and the back transfer process, which finally determines the intensity of the emission of the lanthanide ion.<sup>10</sup> All the work done in this respect in solution has permitted researchers to obtain responsive lanthanide probes for cellular applications.<sup>11,12</sup>

In particular, luminescent compounds containing Tb<sup>III</sup> ions have awakened great interest in coordination chemistry, mainly because these coordination compounds can exhibit relatively long-lived emissions, with excited-state lifetimes of the order of milliseconds. This emission is principally in the green color region, having potential for applications in the solid state as organic light emitting diodes and photoluminescent materials, among others.<sup>13–15</sup> Since the human eye is especially sensitive

Received: January 3, 2020

Published: April 7, 2020



to green light, the compounds that emit this component become very important. Thus, green emission improves the color point of white light and enhances the overall brightness of display devices.<sup>14</sup>

Since the energy of the excited state of ligands can be modified by the presence of substituents, affecting the energy gap between the triplet state of the corresponding ligand and the emissive state of the Tb<sup>III</sup> ion, the luminescence of the derived complexes can be modulated.<sup>16</sup> In this respect, Shi et al. reported that substituents on the 4-position of pyrazolone ligands modified the emission of the corresponding Eu<sup>III</sup> complexes.<sup>17</sup>

Numerous organic ligands have been used in coordination chemistry as luminescent sensitizers.<sup>14,18,19</sup> Among these, pyridylaminophenol ligands, which have shown flexible coordination properties toward transition-metal ions can be also considered as potential sensitizers for lanthanide(III) ions.<sup>20,21</sup>

The goal of the present work was to investigate the photophysical characterization of novel terbium(III) complexes, with substituted tripodal ligands, i.e., 2,2'-[[2-(pyridinylmethyl)-imino]di(methylene)]-bis(4-R-phenol) with R = CH<sub>3</sub> (L<sup>CH<sub>3</sub></sup>), Cl (L<sup>Cl</sup>) and CH<sub>3</sub>O (L<sup>CH<sub>3</sub>O</sup>), COOCH<sub>3</sub> (L<sup>COOCH<sub>3</sub></sup>). The photophysical properties in the solid state of these complexes were studied, and the effect of the substituents on their luminescence is discussed. The thermal dependence of the emission in the solid state was also explored.

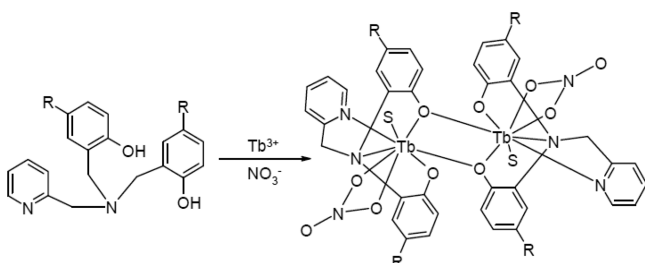
## EXPERIMENTAL SECTION

**Materials and Reagents.** Reagent grade chemicals and HPLC quality solvents were used as received.

**Synthesis of Ligands.** The ligands were prepared as described previously.<sup>20,21</sup>

**Synthesis of Terbium(III) Complexes.** A solution of Tb(H<sub>2</sub>O)<sub>9</sub>(NO<sub>3</sub>)<sub>3</sub> (1 mmol) in 5 mL of MeOH was added with stirring at room temperature to a solution of the corresponding ligand (0.5 mmol) and 1 mmol of MeONa in 20 mL of MeOH. The corresponding solid complexes were separated after 5 to 15 days, in 50% to 70% yield. Recrystallization of the crude products in hot DMF afforded [Tb<sub>2</sub>L<sub>2</sub>(NO<sub>3</sub>)<sub>2</sub>(DMF)<sub>2</sub>] $\cdot$ *x*DMF (L<sup>CH<sub>3</sub></sup> = I, *x* = 2; L<sup>Cl</sup> = II, *x* = 2; L<sup>CH<sub>3</sub>O</sup> = III, *x* = 0; and L<sup>COOCH<sub>3</sub></sup> = IV, *x* = 2) (Scheme 1).

**Scheme 1. Syntheses of Dinuclear Tb<sup>III</sup> Complexes**



[Tb<sub>2</sub>(L<sup>CH<sub>3</sub></sup>)<sub>2</sub>(NO<sub>3</sub>)<sub>2</sub>(DMF)<sub>2</sub>] $\cdot$ 2DMF (I). (C<sub>50</sub>H<sub>54</sub>N<sub>8</sub>O<sub>12</sub>Tb<sub>2</sub>·2(C<sub>3</sub>H<sub>7</sub>NO)). Elemental analysis experimentally determined (calcd) for C<sub>56</sub>H<sub>68</sub>N<sub>10</sub>O<sub>14</sub>Tb<sub>2</sub>: C 47.2 (47.22); H 5.1 (4.82); N 10.2 (9.84)%. FTIR (ATR): 1670, 1650 (ν<sub>C=O DMF</sub>), 1606 (ν<sub>C=Carom</sub>), 1493, 1302 (ν<sub>NO<sub>3</sub></sub>), 1254 (ν<sub>C-O</sub>) cm<sup>-1</sup>.

[Tb<sub>2</sub>(L<sup>Cl</sup>)<sub>2</sub>(NO<sub>3</sub>)<sub>2</sub>(DMF)<sub>2</sub>] $\cdot$ 2DMF (II). (C<sub>46</sub>H<sub>46</sub>Cl<sub>4</sub>N<sub>8</sub>O<sub>12</sub>Tb<sub>2</sub>·2(C<sub>3</sub>H<sub>7</sub>NO)). Elemental analysis exp. determined (calcd) for C<sub>52</sub>H<sub>60</sub>N<sub>10</sub>O<sub>14</sub>C<sub>14</sub>Tb<sub>2</sub>: C 42.1 (41.4); H 3.9 (4.01); N 9.1 (9.28)%. FTIR (ATR): 1669, 1648 (ν<sub>C=O DMF</sub>), 1604 (ν<sub>C=Carom</sub>), 1471, 1286 (ν<sub>NO<sub>3</sub></sub>), 1256 (ν<sub>C-O</sub>) cm<sup>-1</sup>.

[Tb<sub>2</sub>(L<sup>CH<sub>3</sub>O</sup>)<sub>2</sub>(NO<sub>3</sub>)<sub>2</sub>(DMF)<sub>2</sub>] (III). (C<sub>50</sub>H<sub>58</sub>N<sub>8</sub>O<sub>16</sub>Tb<sub>2</sub>). Elemental analysis exp. determined (calcd) for C<sub>50</sub>H<sub>58</sub>N<sub>8</sub>O<sub>16</sub>Tb<sub>2</sub>: C 44.6 (44.65); H 4.5 (4.35); N 8.1 (8.33)%. FTIR (ATR): 1646 (ν<sub>C=ODMF</sub>), 1606 (ν<sub>C=Carom</sub>), 1488, 1300 (ν<sub>NO<sub>3</sub></sub>), 1266 (ν<sub>C-O</sub>) cm<sup>-1</sup>.

[Tb<sub>2</sub>(L<sup>COOCH<sub>3</sub></sup>)<sub>2</sub>(NO<sub>3</sub>)<sub>2</sub>(DMF)<sub>2</sub>] $\cdot$ 2DMF (IV). (C<sub>54</sub>H<sub>58</sub>N<sub>8</sub>O<sub>20</sub>Tb<sub>2</sub>·2(C<sub>3</sub>H<sub>7</sub>NO)). Elemental analysis exp. determined (calcd) for C<sub>60</sub>H<sub>72</sub>N<sub>10</sub>O<sub>22</sub>Tb<sub>2</sub>: C 44.6 (44.95); H 4.4 (4.53); N 8.5 (8.74)%. FTIR (ATR): 1700 (ν<sub>C=O</sub>), 1670, 1650 (ν<sub>C=O DMF</sub>), 1600 (ν<sub>C=Carom</sub>), 1490, 1285 (ν<sub>NO<sub>3</sub></sub>), 1260 (ν<sub>C-O</sub>) cm<sup>-1</sup>.

**Synthesis of Yttrium(III) Complexes.** All Y<sup>III</sup> complexes were prepared using a similar method employed for the synthesis of the Tb<sup>III</sup> complexes. The syntheses of corresponding Y<sup>III</sup> complexes are given as Supporting Information.

**Physical Measurements.** Elemental C, H, and N analyses were carried out with Flash 2000 equipment. Fourier transform infrared spectra (FTIR) in the range of 4000 to 400 cm<sup>-1</sup> were obtained using a Thermo Scientific Nicolet iS5 instrument, with an ATR iD5 accessory. <sup>1</sup>H NMR spectra were recorded in CDCl<sub>3</sub> or DMSO-d<sub>6</sub> on a Bruker AMX-300 NMR spectrometer. Chemical shifts are reported as δ values downfield of an internal Me<sub>4</sub>Si reference. Crystal structures were resolved by X-ray diffraction using a SMART-APEX II CCD diffractometer. Reduction of the data was done with SAINT.<sup>22</sup> SADAB<sup>23</sup> was applied for empirical or numerical absorption corrections. Structure solution was done by direct methods and completion using difference Fourier synthesis, while refinement was made by least-squares using SHELXL.<sup>24</sup> The positions of the hydrogen atoms were calculated after each refinement cycle with SHELXL using a riding model for every structure, taking the C—H distance as 0.93, 0.96, or 0.97 Å. For these cases the values of U<sub>iso</sub>(H) were adjusted to 1.2U<sub>eq</sub> or 1.5U<sub>eq</sub> of the parent carbon atom. A summary of the structural and refinement details for the studied complexes is given in Table S1.

The diffuse reflectance spectra (DRS) were obtained using PerkinElmer Lambda WB1050 equipment with a Praying Mantis diffuse reflection accessory. A Horiba–Jobin–Yvon spectrofluorimeter, model Fluorolog-3 (FL3-221), equipped with a 450 W Xe lamp as an excitation source and a Horiba PPD-850 ps photon detector operating in the UV–vis region were used in all photoluminescence (PL) measurements. The luminescence decay curves were measured using a Xe-pulse lamp under an excitation at 325 nm. In all measurements the slits used were 1.5 nm. Both temperature-dependent PL spectra and decay curves were registered using a closed-cycle cryostat model CS202AI-X15 (ARS Cryo) in combination with a temperature Lake Shore model 332 controller. Quantum yield (QY) of the Tb<sup>III</sup> luminescence for all complexes was measured using a 152 mm integrating sphere (Quanta-φ equipment, F3029, Horiba–Jobin–Yvon) of Spectralon coupled by means of optical fibers. The sample holder and reflection standard were also made of Spectralon. The internal and external QY's (Φ's) were calculated following the method developed by Wrighton et al.<sup>25</sup> The internal QY was calculated according to the given equation: Φ<sub>int</sub> (%) = (E<sub>s</sub> / (R<sub>std</sub> - R<sub>s</sub>)) × 100, where E<sub>s</sub> is the number of emitted photons from the sample and R<sub>std</sub> and R<sub>s</sub> are the number of reflected photons from the reflection standard and from the sample, respectively, with (R<sub>std</sub> - R<sub>s</sub>) being the number of photons absorbed by the sample. The external QY (Φ<sub>ext</sub> (%) = E<sub>s</sub> / R<sub>std</sub> × 100) is the ratio between the number of emitted photons from the sample and the number of reflected photons from the reflection standard, i.e., the total number of photons incident over the sample. PL spectra were corrected for the spectral response of the integrating sphere, the monochromators, and the detector using a typical correction spectrum provided by the manufacturer.<sup>26</sup> The FluorEssence ver. 3.5 software was employed to determine the PL quantum yields (Φ<sub>int</sub> and Φ<sub>ext</sub>) and the emission color coordinate values. All optical measurements were recorded using finely ground powder samples. The Commission International d'Éclairage, (CIE 1931) *x,y* coordinates and color diagram were calculated from the photoluminescence spectra using the standard procedures defined by Wyman et al.<sup>27</sup> The correlated color temperature (CCT) was calculated by the McCamy et al. formula:<sup>28</sup> CCT = -437n<sup>3</sup> + 360n<sup>2</sup> - 6861n + 5514.31, where n = (x - x<sub>c</sub>) / (y -

$y_c$ ), where  $x$  and  $y$  are the chromaticity coordinates;  $x_c = 0.3320$  and  $y_c = 0.1858$  are the coordinates of the chromaticity epicenter.

## RESULTS AND DISCUSSION

**Structural Characterization.** The detailed crystallographic data and structure refinement parameters for I–IV are given in Table S1. I–IV crystallize in the orthorhombic (*Pbca*), triclinic (*P1*), monoclinic (*P2<sub>1</sub>/n*), and triclinic (*P1*) space groups. II exhibits two very similar molecules of the complex but crystallographically nonequivalent labeled II-1 and II-2. All the other crystal structures display only one crystallographic moiety. For the complete series of complexes, each terbium(III) center is octa-coordinated. The coordination sphere of the Tb<sup>III</sup> centers is formed by one amine and one pyridyl nitrogen atom, three phenoxo oxygens from the pyridylaminophenol ligands, one solvate oxygen from *N,N'*-dimethylformamide, and a bidentate nitrate. Using SHAPE calculations, the coordination geometry around the Tb<sup>III</sup> ion for all the studied complexes was assessed to be a triangular dodecahedron (Table S2). Figure 1 for IV and Figure S1 for I, II, and III show the ORTEP diagrams for the reported complexes.

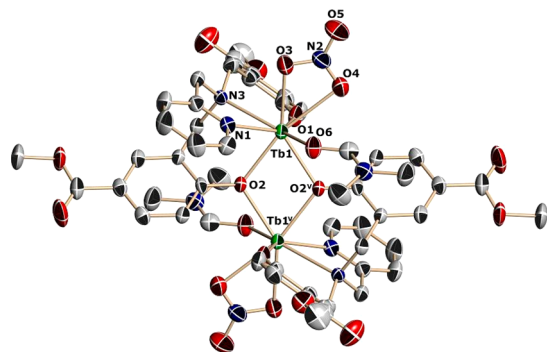


**Figure 1.** Molecular structure diagram for  $[\text{Tb}_2(\text{L}^{\text{COOCH}_3})_2(\text{NO}_3)_2(\text{DMF})_2] \cdot 2\text{DMF}$  (IV). Atoms at the 50% level of probability. Hydrogen atoms have been omitted for clarity.

All the dinuclear species are assembled around a central and regular  $\text{Tb}_2\text{O}_2$  parallelogram, with a  $\mu$ -bridging phenoxo oxygen atom from each ligand. The molecular point group is  $C_i$  due to the existence of an inversion center in the middle of the parallelogram that is, therefore, strictly planar. The central parallelogram and the phenolate group define a dihedral angle of  $50.22(9)^\circ$  (I),  $47.8(1)^\circ$  (II-1),  $45.6(2)^\circ$  (II-2),  $44.8(2)^\circ$  (III), and  $46.7(2)^\circ$  (IV). Table 1 gives a summary of the most relevant bond distances and angles for IV, while Table S3 shows the same parameters for the complete series of complexes.

**Optical Properties.** Solid-state diffuse reflectance spectra of Tb<sup>III</sup> and Y<sup>III</sup> complexes are given as Supporting Information (Figures S2 and S3). The emission properties of the complexes were studied in the solid state and are discussed below. Figure 2a depicts the excitation spectra of I–IV at room temperature by monitoring the emission band at 546 nm. This consists of a broad band spanning from 300 to 410 nm, which can be attributed to the  $S_0$  to  $S_1$  transition of the ligands.<sup>21</sup> The  ${}^7\text{F}_6 \rightarrow {}^5\text{D}_4$  transition centered at 486 nm is also observed.

Figure 2b shows the emission spectra of I–IV at room temperature. It consists of four distinct bands centered at 490, 546, 585, and 620 nm, assigned to the  ${}^5\text{D}_4 \rightarrow {}^7\text{F}_6$ ,  ${}^5\text{D}_4 \rightarrow {}^7\text{F}_5$ ,

**Table 1.** Selected Interatomic, Bond Distances, and Angles for  $\text{Tb}_2(\text{L}^{\text{COOCH}_3})_2(\text{NO}_3)_2(\text{DMF})_2 \cdot 2\text{DMF}$  (IV)<sup>a</sup>

Tb1—O1	2.167(3)	Tb1—O4	2.549(3)
Tb1—O2	2.320(3)	Tb1—N3	2.567(3)
Tb1—O2	2.372(3)	Tb1...Tb1 <sup>v</sup>	3.8462(5)
Tb1—O6	2.411(3)	O1—C1	1.312(5)
Tb1—O3	2.451(4)	O2—C9	1.342(5)
Tb1—N1	2.507(4)	O2—Tb1 <sup>v</sup>	2.372(3)
O1—Tb1—O2	100.60(11)	O3—Tb1—N1	72.91(12)
O1—Tb1—O2 <sup>v</sup>	84.00(11)	O1—Tb1—O4	77.51(12)
O2—Tb1—O2 <sup>v</sup>	69.87(11)	O2—Tb1—O4	164.81(11)
O1—Tb1—O6	139.96(11)	O2 <sup>v</sup> —Tb1—O4	94.95(11)
O2—Tb1—O6	103.01(11)	O6—Tb1—O4	71.29(11)
O2 <sup>i</sup> —Tb1—O6	74.53(11)	O3—Tb1—O4	50.54(11)
O1—Tb1—O3	96.73(13)	N1—Tb1—O4	117.15(12)
O2—Tb1—O3	144.04(11)	O1—Tb1—N3	73.82(11)
O2 <sup>v</sup> —Tb1—O3	143.70(11)	O2—Tb1—N3	78.61(11)
O6—Tb1—O3	82.47(12)	O2 <sup>v</sup> —Tb1—N3	137.11(11)
O1—Tb1—N1	141.14(12)	O6—Tb1—N3	142.52(11)
O2—Tb1—N1	73.84(11)	O3—Tb1—N3	76.34(12)
O2 <sup>v</sup> —Tb1—N1	126.57(11)	N1—Tb1—N3	67.36(12)
O6—Tb1—N1	77.07(12)	O4—Tb1—N3	114.70(12)
Tb1—O2—Tb1 <sup>v</sup>	110.13(11)		

<sup>a</sup>Symmetry label:  $v = -x, -y + 2, -z$ .

${}^5\text{D}_4 \rightarrow {}^7\text{F}_4$ , and  ${}^5\text{D}_4 \rightarrow {}^7\text{F}_3$  transitions of the Tb<sup>III</sup> ions. The  ${}^5\text{D}_4 \rightarrow {}^7\text{F}_5$  green transition (magnetic dipole character, MD) is the most intense and presents the same Stark splitting, position, and line width for all complexes. These features indicate that Tb<sup>III</sup> occupies a similar site symmetry environment in all the studied complexes as evidenced by the X-ray structure characterization. It is evident that the substituent on the phenol moiety affects the intensity of the emission of the metal ion. It is important to note that the complex with the ligand having the strong electron accepting  $\text{COOCH}_3$  group has the most intense emission, while that with the strong electron donating  $\text{CH}_3\text{O}$  group has the less intense emission. This effect can be attributed to the capacity of the substituent to stabilize the coordinated phenoxo group, modulating the energy gap between the triplet state of the ligand and the emissive state of Tb<sup>III</sup>.<sup>16</sup>

No emission arising from the ligands could be detected, indicating an efficient ligand-to-Tb<sup>III</sup> energy transfer.<sup>29</sup> Since Y<sup>III</sup> ions are not luminescent, the corresponding spectra were used to distinguish the emission bands of the ligands.<sup>30</sup> Figure S4 shows the emission spectra of the Y<sup>III</sup> complexes. The calculated energies of the triplet and singlet excited states for VIII,  $T_1$  and  $S_1$ , of  $\text{L}^{\text{COOCH}_3}$  are 423 nm ( $23640 \text{ cm}^{-1}$ ) and 342 nm ( $29240 \text{ cm}^{-1}$ ), respectively; the corresponding energy values for V–VII were recently published.<sup>20</sup>

It is well established that for an efficient ligand-to-metal energy transfer, the energy gap ( $\Delta E$ ) between the triplet excited state ( $T_1$ ) and the excited state of Tb<sup>III</sup> ions,  $\Delta E[T_1 - {}^5\text{D}_4]$ , should be between  $1850\text{--}4500 \text{ cm}^{-1}$ , in order to minimize back transfer. For I–IV, the  $\Delta E$  values were estimated as 1758, 2657, 330, and  $3140 \text{ cm}^{-1}$ , respectively. As the estimated  $\Delta E$  for III is smaller than the optimal ligand-to-metal energy gap value, the observed low emission of this complex is justified.<sup>16,31</sup>

**Photoluminescence versus Temperature.** Temperature-dependent luminescence experiments were performed in order to study the thermal behavior of the emission intensity

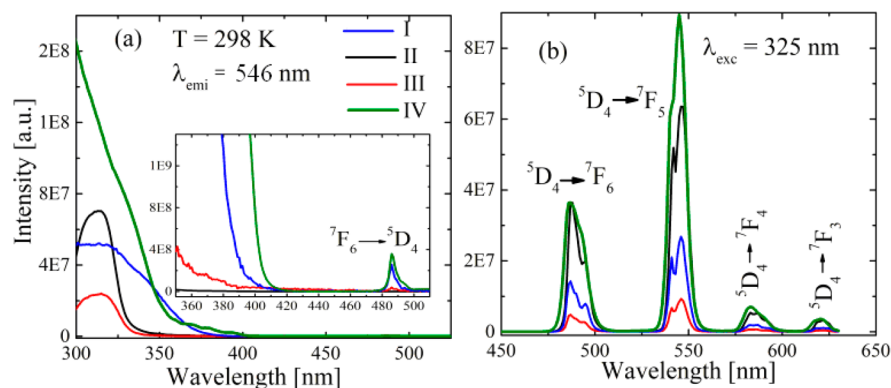


**Figure 2.** (a) Tb<sup>III</sup> excitation spectra monitoring the  $^5D_4 \rightarrow ^7F_5$  transition at 546 nm. The inset in (a) shows the excitation of  $^7F_6 \rightarrow ^5D_4$  transition centered at 486 nm. (b) Emission spectra for I–IV upon excitation at 325 nm (room temperature).

of the Tb<sup>III</sup> complexes. Figure 3 shows the temperature dependence of the emission spectra in the 15–300 K range for

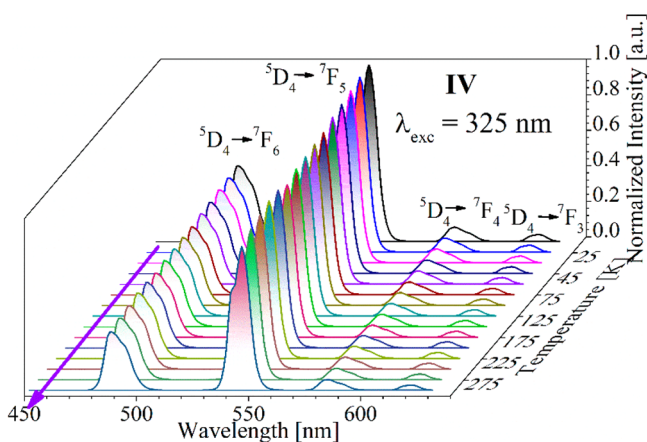


**Figure 3.** Tb<sup>III</sup> emission spectra under excitation at 325 nm as a function of the temperature for IV.

IV, normalized with respect to the  $^5D_4 \rightarrow ^7F_5$  transition intensity. Similar spectra recorded for I, II, and III are depicted in Figure S5. In all cases, the bands become more intense as the temperature is decreased. As reported by Ramesh et al.,<sup>32</sup> the decrease of the intensity of the emission with the increase in temperature is due to nonradiative relaxation through thermal activation via the crossing point between the ground and excited states.

The dominant emission is always that corresponding to the  $^5D_4 \rightarrow ^7F_5$  transition. The  $^5D_4 \rightarrow ^7F_{2,1}$  transitions could not be detected experimentally because these lie at lower energies, out of the recorded region. Emission from the  $^5D_3$  state was not observed in the spectra, even at low temperatures.<sup>33,34</sup> As shown in Figures 3 and S5a–c the barycenter of the observed Tb<sup>III</sup> transitions is temperature independent, within experimental error. Lowering the temperature, the Stark splitting pattern of the observed transitions remains unaltered.

The  $^5D_4 \rightarrow ^7F_5$  transition at 546 nm (green, G) has a magnetic dipole nature (MD) and is not affected by the ligand environment. Therefore, it can be used as an internal reference compared to the  $^5D_4 \rightarrow ^7F_6$  transition at 486 nm (blue, B), which is sensitive to the ligand environment and to the coordination site symmetry.<sup>35</sup> So, the ratio of these two transitions was used as a measurement of the local site symmetry of the Tb<sup>III</sup> coordination environment. Figure 4a–d

shows the temperature dependence of the integrated intensities of  $^5D_4 \rightarrow ^7F_5$  and  $^5D_4 \rightarrow ^7F_6$  transitions, the  $G/B = I(^5D_4 \rightarrow ^7F_5)/I(^5D_4 \rightarrow ^7F_6)$  ratio, as well as the total normalized integrated intensity  $I/I_{15K}$ . In Figures 4a and 4b, the two monitored transitions for a given complex have the same thermal behavior. Quenching of Tb<sup>III</sup> luminescence is observed with the increase of temperature. In the range between 15 K to ca. 50 K, I, II, and IV show a slight decrease, while for III this is more pronounced. Above 150 K, the emission of II and IV remains almost constant until room temperature. However, for I there is a slight decrease, while III shows a pronounced decrease, becoming the less emissive at room temperature. At room temperature the sequence of intensities is IV > II > I > III.

As pointed by Linganna et al.<sup>36</sup> the Tb<sup>III</sup> G/B ratio plays the role of describing the covalent/ionic character bonding between the Tb<sup>III</sup> and oxygen atom.<sup>37</sup> Our results (Figure 4c) show that the G/B ratio remains almost constant for all complexes with the increase of the temperature, suggesting that the degree of covalence for Tb<sup>III</sup>–oxygen bonds does not change with temperature.

In Figure 4d, the normalized total integrated intensity ( $I/I_{15K}$ ) was evaluated from the photoluminescence curve in the spectral range of 450 to 630 nm of all complexes. The fitting of the experimental emission data with increasing temperature was best done using the Mott–Seitz model considering two deactivation processes.<sup>38</sup>

$$I_T = I_{15K} / (1 + C_1 \exp(-\Delta E_{A1}/kT) + C_2 \exp(-\Delta E_{A2}/kT)) \quad (1)$$

where  $I_{15K}$  and  $I_T$  are the emission intensities at 15 K and  $T$  K,  $C_i$  is the ratio between the nonradiative and radiative probabilities, and  $\Delta E_{Ai}$  is the activation energy required to activate the corresponding thermal quenching process.

The thermal dependence can be understood in terms of the calculated  $C$  and  $\Delta E$  parameters. Up to ca. 50 K, all complexes show a similar behavior which can be rationalized by similar  $C_1$  and  $\Delta E_{A1}$ , operating at low temperatures. Above 50 K, a temperature dependence is observed for complexes I and III. These complexes present the higher  $C_2$  values, which can explain the decrease in the intensity. Furthermore, complex III has a low energy barrier,  $\Delta E_{A2}$ , which also determines the low intensity at room temperature. The intensity for II and IV are almost independent of temperature above 50 K. For II the low energy barrier should facilitate the nonradiative process, but

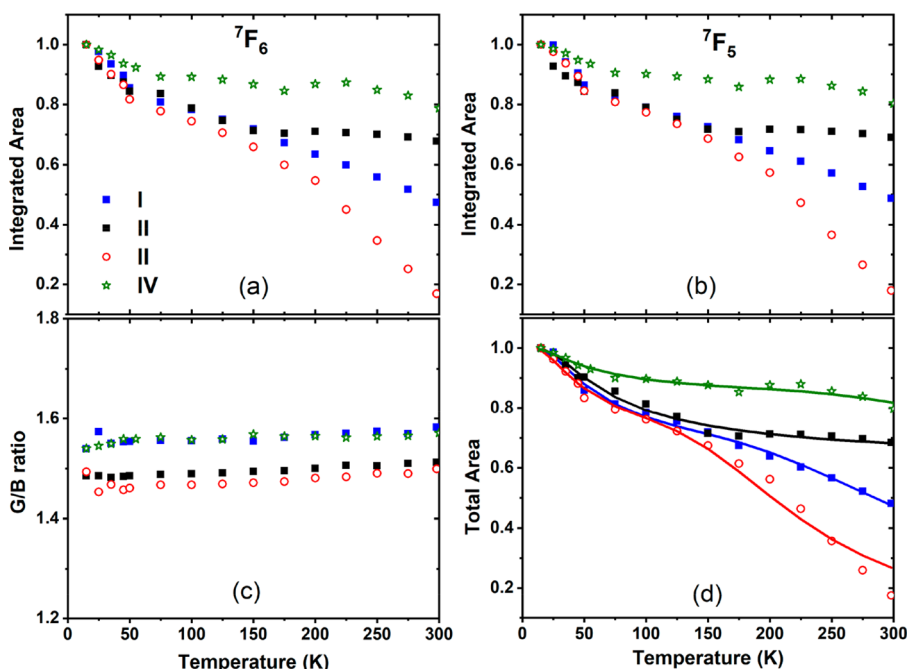


**Figure 4.** Variation of the integrated area of luminescence intensities against the temperature in I (blue), II (black), III (red), and IV (green): (a) for  ${}^5\text{D}_4 \rightarrow {}^7\text{F}_6$  (B) and (b) for  ${}^5\text{D}_4 \rightarrow {}^7\text{F}_5$  (G) transitions, (c) G/B ratio, and (d) total normalized integrated intensity,  $I/I_{SK}$ , as a function of the temperature. The solid lines in (d) corresponds to the fitting of the experimental data using the Mott–Seitz model.

the low  $C_2$  value indicates that the dominant pathway should be the radiative one. For IV, despite of the high  $C_2$  value, the very high energy barrier explains the stable intensity at high temperature (Table 2).

**Table 2. Fitting Parameters for the Thermal Dependence of the Total Integrated Intensity**

complex	I	II	III	IV
substituent	CH <sub>3</sub>	Cl	CH <sub>3</sub> O	COOCH <sub>3</sub>
$C_1$	0.68	0.53	0.57	0.21
$\Delta E_{A1}$ , eV	0.007	0.008	0.006	0.005
$\Delta E_{A1}$ , cm <sup>-1</sup>	55	61	45	41
$C_2$	30	0.0928	39	19
$\Delta E_{A2}$ , eV	0.1	0.007	0.073	0.153
$\Delta E_{A2}$ , cm <sup>-1</sup>	810	58	59	1239

**Photoluminescence Lifetimes Results and Sensitization.** Figure 5 depicts the results for the emission decay

analysis of IV; the photoluminescence was excited with a pulsed light with  $\lambda_{exc} = 325$  nm, and the decay was obtained monitoring the intense  ${}^5\text{D}_4 \rightarrow {}^7\text{F}_5$  green emission at 546 nm. A monoexponential function gave the best fit for II and IV, while the decay curves for I and III were fitted with a biexponential function:<sup>39</sup>

$$I(t)/I_0 = A_1 \exp(-t/\tau_1) + A_2 \exp(-t/\tau_2) \quad (2)$$

where  $A_1$  and  $A_2$  are constants,  $\tau_1$  and  $\tau_2$  the decay time for the exponential component, and  $I(t)/I_0$  the normalized intensity. The average lifetime for I and III was calculated by using eq 3:

$$\tau_{AV} = \frac{A_1\tau_1^2 + A_2\tau_2^2}{A_1\tau_1 + A_2\tau_2} \quad (3)$$

with the  $\tau$  and  $A$  values of each component at 15 and 300 K are given in Table 3. The values for other temperatures are given in Tables S4 and S5.

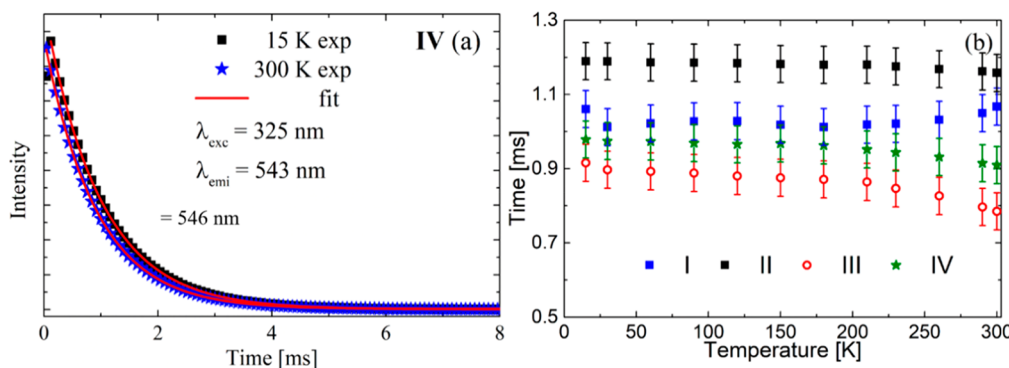


**Figure 5.** (a) Decay curves of IV at 15 and 300 K. (b) Thermal dependence of the average emission lifetime of the Tb<sup>III</sup>  ${}^5\text{D}_4 \rightarrow {}^7\text{F}_5$  transition for I–IV ( $\lambda_{exc} = 325$  nm;  $\lambda_{emi} = 546$  nm).

Table 3. Photometric Parameters<sup>a</sup>

complex	$\Phi_{\text{int}}$ (%)	$\Phi_{\text{ext}}$ (%)	$T$ (K)	$\tau_1$ (ms) ( $A_1$ )	$\tau_2$ (ms) ( $A_2$ )	$\tau_{\text{av}}$ (ms)	CIE	CCT (K)	CP (%)
I	5.9(6)	3.9(4)	15	1.22(5)	0.48(5)	1.06(5)	(0.289, 0.596)	6274(63)	94
			300	1.18(5)	0.36(5)	1.07(5)	(0.289, 0.597)	6275(63)	95
II	16.5(9)	10.6(9)	15	1.19(5)			(0.275, 0.564)	6622(66)	85
			300	1.16(5)			(0.275, 0.562)	6633(66)	84
III	2.1(2)	0.4(1)	15	1.07(5)	0.34(5)	0.92(5)	(0.285, 0.597)	6355(64)	98
			300	0.85(5)	0.11(5)	0.78(5)	(0.282, 0.596)	6398(64)	98
IV	17.7(8)	13.0(9)	15	0.98(5)			(0.283, 0.597)	6378(64)	98
			300	0.91(5)			(0.287, 0.598)	6387(64)	99

<sup>a</sup>PLQY,  $\Phi$ ; decay lifetime,  $\tau$ ; CIE ( $x, y$ ) coordinates; CCT (K) and color purity (CP) values for all complexes ( $\lambda_{\text{exc}} = 325$  nm;  $\lambda_{\text{emi}} = 546$  nm).

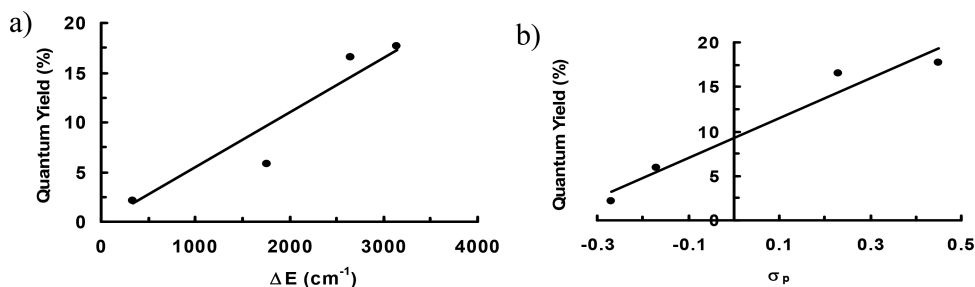


Figure 6. (a) Dependence of the quantum yield with the energy gap ( $\Delta E$ ) and (b) with the Hammett parameter,  $\sigma_p$ .

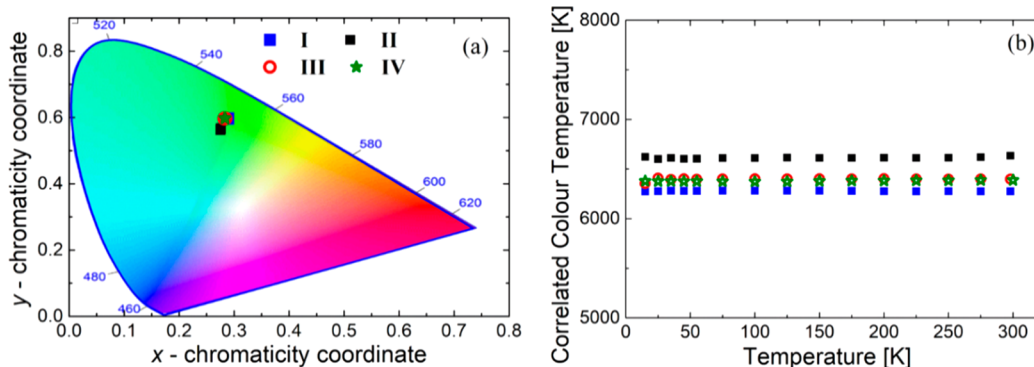


Figure 7. Thermal dependence of (a) CIE 1931 chromaticity coordinate diagram for I–IV and (b) the CCT values.

Figure 5b clearly shows that no significant dependence of the  $\tau_{\text{av}}$  with temperature can be observed; the small changes are within the experimental error. The longer lifetime  $\tau_1$  observed for the four complexes must be related to the sensitized emission of the  $\text{Tb}^{\text{III}}$  ion. The biexponential decay for I and III is indicative that in these complexes two energy processes are involved in the observed emissions, one of which should be related to the presence of back-energy transfer from the metal center. The back-energy transfer in I and III can be justified by the small calculated energy gap values ( $\Delta E$ ). Furthermore, the obtained  $\tau$  values for our complexes are within the range of those reported for other  $\text{Tb}^{\text{III}}$  complexes.<sup>40–42</sup>

In order to best quantify the influence of the substituent on the luminescence efficiency of I–IV, the internal and external quantum yields ( $\Phi_{\text{int}}$  and  $\Phi_{\text{ext}}$ ) were calculated<sup>17,18</sup> and are presented in Table 3. The results indicate that the values follow the trend  $\text{IV} > \text{II} \gg \text{I} > \text{III}$ , in accordance with the

effect of the decrease of the electron withdrawing effect of the substituent on the emission, as reported in the literature.<sup>16,17</sup> These values, together with the estimated energy gap ( $\Delta E$ ) between the triplet excited state ( $T_1$ ) and the emissive state  $^5D_4$  of  $\text{Tb}^{\text{III}}$  ions (1758, 2657, 330, and 3140  $\text{cm}^{-1}$  for I, II, III, and IV, respectively) show a clear effect of the substituents on the luminescent properties of the studied complexes. Figure 6a shows a linear dependence of the quantum yield with the values of the estimated energy gap ( $\Delta E$ ). Quantum yields can also be correlated with the inductive Hammett parameter  $\sigma_p$  for the used *para*-substituents (Figure 6b).<sup>43</sup>

All these findings agree with that reported by Latva et al.,<sup>44</sup> who extensively studied the correlation between the lowest triplet energy level of 41 ligands and the emitting energy level of  $\text{Tb}^{\text{III}}$  ions, showing that increasing  $\Delta E$  increases the luminescence quantum yield. Nevertheless, a correlation between the effect of the substituent and the lifetime of the studied complexes was not observed.

**CIE, CCT, and CP Parameters.** Figure 7a shows the color diagram for the studied complexes. For all Tb<sup>III</sup> complexes, the CIE 1931 values do not shift with the temperature, lying in the green region; the values being (0.289, 0.596), (0.275, 0.564), (0.285, 0.597), and (0.283, 0.597) at 15 K and (0.289, 0.597), (0.275, 0.562), (0.282, 0.596), and (0.287, 0.598) at 300 K for I, II, III, and IV, respectively.

Using eq 4, the color purity (CP) was calculated:<sup>45</sup>

$$CP = \sqrt{\frac{(x - x_i)^2 + (y - y_i)^2}{(x_d - x_i)^2 + (y_d - y_i)^2}} \times 100\% \quad (4)$$

where (x,y) are the color coordinates of the overall light emitted by I–IV (Figure 7a), together with the standard white light value, (x<sub>w</sub>,y<sub>w</sub>) = (0.333, 0.333), and the dominant wavelength point for green color (x<sub>d</sub>,y<sub>d</sub>) = (0.290, 0.600). The estimated CP for I–IV are impressive, at 95%, 84%, 98%, and 99%, respectively, both at 15 K and at room temperature.

The correlated color temperature (CCT) values as a function of the temperature, calculated using the McCamy formula,<sup>28</sup> for I–IV are presented in Figure 7b. Since the CCT values are constant, i.e., 6275, 6633, 6398, and 6387 K for I, II, III, and IV, respectively, and are greater than 5000 K, these complexes can be considered suitable for the improvement of the color point of white light and, thus, the enhancement of the overall brightness of display devices.

## CONCLUSIONS

The dinuclear Tb<sup>III</sup> complexes based on the tripodal ligands 2,2'-[[2-(pyridinylmethyl)imino]di(methylene)]-bis(4-R-phenol), where R = CH<sub>3</sub> (I), Cl (II), CH<sub>3</sub>O (III), and COOCH<sub>3</sub> (IV), were shown to exhibit luminescent properties. The intensity of the emission bands is greatly affected by the nature of the substituent on the phenoxo moiety. The COOCH<sub>3</sub> substituent enhances the intensity of the emission by a factor of ca. 10, as compared to that of CH<sub>3</sub>O. Besides, the following order for the quantum yield was observed: IV > II ≫ I > III, indicating that the best sensitizer is the ligand substituted with –COOCH<sub>3</sub>. The quantum yield shows a linear dependence with the energy gap ΔE and the Hammett parameter, σ<sub>p</sub>. Of the obtained complexes, IV may be considered as appropriate for applications in light-emitting diodes (OLEDs), since the CCT value lies ca. 6400 K, and the CP is 99% at room temperature.

## ASSOCIATED CONTENT

### Supporting Information

The Supporting Information is available free of charge at <https://pubs.acs.org/doi/10.1021/acs.inorgchem.0c00023>.

Synthesis, characterization, diffuse reflectance spectra, emission spectra, X-ray data, and SHAPE calculations (PDF)

### Accession Codes

CCDC 1972883–1972885 and 1972888 contain the supplementary crystallographic data for this paper. These data can be obtained free of charge via [www.ccdc.cam.ac.uk/data\\_request/cif](http://www.ccdc.cam.ac.uk/data_request/cif), or by emailing [data\\_request@ccdc.cam.ac.uk](mailto:data_request@ccdc.cam.ac.uk), or by contacting The Cambridge Crystallographic Data Centre, 12 Union Road, Cambridge CB2 1EZ, UK; fax: +44 1223 336033.

## AUTHOR INFORMATION

### Corresponding Authors

**Jorge Manzur** – Facultad de Ciencias Físicas y Matemáticas, Universidad de Chile, Santiago, Chile; Email: [jmanzur@ing.uchile.cl](mailto:jmanzur@ing.uchile.cl)

**Ricardo Costa de Santana** – Instituto de Física, Universidade Federal de Goiás, Goiânia (GO), Brazil; [orcid.org/0000-0002-6484-7484](https://orcid.org/0000-0002-6484-7484); Email: [santana@ufg.br](mailto:santana@ufg.br)

**Evgenia Spodine** – Facultad de Ciencias Químicas y Farmacéuticas, Universidad de Chile, Santiago, Chile; Centro para el Desarrollo de Nanociencias y Nanotecnología, CEDENNA, Santiago, Chile; Email: [espodine@uchile.cl](mailto:espodine@uchile.cl)

### Authors

**Carolina Poblete** – Facultad de Ciencias Físicas y Matemáticas, Universidad de Chile, Santiago, Chile

**Jeannette Morales** – Facultad de Ciencias Químicas y Farmacéuticas, Universidad de Chile, Santiago, Chile

**Lauro June Queiroz Maia** – Instituto de Física, Universidade Federal de Goiás, Goiânia (GO), Brazil

**Andres Vega** – Departamento de Ciencias Químicas, Universidad Andrés Bello, Santiago, Chile; Centro para el Desarrollo de Nanociencias y Nanotecnología, CEDENNA, Santiago, Chile; [orcid.org/0000-0001-6501-4161](https://orcid.org/0000-0001-6501-4161)

**Pablo Fuentealba** – Facultad de Ciencias Químicas y Farmacéuticas, Universidad de Chile, Santiago, Chile; Centro para el Desarrollo de Nanociencias y Nanotecnología, CEDENNA, Santiago, Chile

Complete contact information is available at:

<https://pubs.acs.org/doi/10.1021/acs.inorgchem.0c00023>

### Author Contributions

The manuscript was written through contributions of all authors. All authors have given approval to the final version of the manuscript.

### Notes

The authors declare no competing financial interest.

## ACKNOWLEDGMENTS

E.S. and J.M.R. acknowledge financial support from the FONDECYT 1160106 grant. E.S., P.F., and A.V. thank Financiamiento Basal AFB 180001 (CEDENNA) for support. This study was financed in part by the Coordenação de Aperfeiçoamento de Pessoal de Nível Superior (CAPES), Conselho Nacional de Desenvolvimento Científico e Tecnológico (CNPq), Fundação de Amparo à Pesquisa do Estado de Goiás (FAPEG), and Financiadora de Estudos e Projetos (FINEP) Brazilian agencies.

## REFERENCES

- Bünzli, J.-C. G.; Piguet, C. Taking Advantage of Luminescent Lanthanide Ions. *Chem. Soc. Rev.* **2005**, *34* (12), 1048.
- Bünzli, J.-C. G.; Comby, S.; Chauvin, A.-S.; Vandevyver, C. D. B. New Opportunities for Lanthanide Luminescence. *J. Rare Earths* **2007**, *25* (3), 257–274.
- Carlos, L. D.; Ferreira, R. A. S.; Bermudez, V. de Z.; Ribeiro, S. J. L. Lanthanide-Containing Light-Emitting Organic-Inorganic Hybrids: A Bet on the Future. *Adv. Mater.* **2009**, *21* (5), 509–534.
- Carlos, L. D.; Ferreira, R. A. S.; de Zea Bermudez, V.; Julián-López, B.; Escribano, P. Progress on Lanthanide-Based Organic-Inorganic Hybrid Phosphors. *Chem. Soc. Rev.* **2011**, *40* (2), 536–549.
- Bünzli, J.-C. G. Lanthanide Photonics: Shaping the Nanoworld. *Trends Chem.* **2019**, *1* (8), 751–762.

- (6) Bünzli, J.-C. G.; Eliseeva, S. V. Lanthanide NIR Luminescence for Telecommunications, Bioanalyses and Solar Energy Conversion. *J. Rare Earths* **2010**, *28* (6), 824–842.
- (7) Parker, D.; Williams, J. A. G. Getting Excited about Lanthanide Complexation Chemistry. *J. Chem. Soc., Dalton Trans.* **1996**, No. 18, 3613.
- (8) Shiraishi, Y.; Furubayashi, Y.; Nishimura, G.; Hirai, T. Sensitized Luminescence of Eu and Tb Macrocyclic Complexes Bearing Benzophenone Antennae. *J. Lumin.* **2007**, *126* (1), 68–76.
- (9) Guillaumont, D.; Bazin, H.; Benech, J.-M.; Boyer, M.; Mathis, G. Luminescent Eu(III) and Gd(III) Trisbipyridine Cryptates: Experimental and Theoretical Study of the Substituent Effects. *ChemPhysChem* **2007**, *8* (3), 480–488.
- (10) Chauvin, A.-S.; Comby, S.; Baud, M.; De Piano, C.; Duhot, C.; Bünzli, J.-C. G. Luminescent Lanthanide Helicates Self-Assembled from Ditopic Ligands Bearing Phosphonic Acid or Phosphoester Units. *Inorg. Chem.* **2009**, *48* (22), 10687–10696.
- (11) New, E. J.; Parker, D.; Smith, D. G.; Walton, J. W. Development of Responsive Lanthanide Probes for Cellular Applications. *Curr. Opin. Chem. Biol.* **2010**, *14* (2), 238–246.
- (12) Montgomery, C. P.; Murray, B. S.; New, E. J.; Pal, R.; Parker, D. Cell-Penetrating Metal Complex Optical Probes: Targeted and Responsive Systems Based on Lanthanide Luminescence. *Acc. Chem. Res.* **2009**, *42* (7), 925–937.
- (13) Cui, Y.; Yue, Y.; Qian, G.; Chen, B. Luminescent Functional Metal-Organic Frameworks. *Chem. Rev.* **2012**, *112* (2), 1126–1162.
- (14) Binnemans, K. Lanthanide-Based Luminescent Hybrid Materials. *Chem. Rev.* **2009**, *109* (9), 4283–4374.
- (15) Cui, R.; Liu, W.; Zhou, L.; Zhao, X.; Jiang, Y.; Cui, Y.; Zhu, Q.; Zheng, Y.; Zhang, H. Green Phosphorescent Organic Electroluminescent Devices with 27.9% External Quantum Efficiency by Employing a Terbium Complex as a Co-Dopant. *J. Mater. Chem. C* **2019**, *7* (26), 7953–7958.
- (16) Samuel, A. P. S.; Xu, J.; Raymond, K. N. Predicting Efficient Antenna Ligands for Tb(III) Emission. *Inorg. Chem.* **2009**, *48* (2), 687–698.
- (17) Shi, M.; Li, F.; Yi, T.; Zhang, D.; Hu, H.; Huang, C. Tuning the Triplet Energy Levels of Pyrazolone Ligands to Match the S<sub>0</sub> Level of Europium(III). *Inorg. Chem.* **2005**, *44* (24), 8929–8936.
- (18) de Bettencourt-Dias, A.; Barber, P. S.; Viswanathan, S. Aromatic N-Donor Ligands as Chelators and Sensitizers of Lanthanide Ion Emission. *Coord. Chem. Rev.* **2014**, *273–274*, 165–200.
- (19) D'Aléo, A.; Picot, A.; Beeby, A.; Gareth Williams, J. A.; Le Guennic, B.; Andraud, C.; Maury, O. Efficient Sensitization of Europium, Ytterbium, and Neodymium Functionalized Tris-Dipicolinate Lanthanide Complexes through Tunable Charge-Transfer Excited States. *Inorg. Chem.* **2008**, *47* (22), 10258–10268.
- (20) Manzur, J.; de Santana, R. C.; Maia, L. J. Q.; Vega, A.; Spodine, E. Tuning White Light Emission in Dinuclear Phenoxo Bridged Dy III Complexes. *Inorg. Chem.* **2019**, *58* (15), 10012–10018.
- (21) Davila, R.; Farias, N.; Carolina Sañudo, E.; Vega, A.; Escuer, A.; Soler, M.; Manzur, J. Dinuclear Cobalt(II) and Mixed Valence Trinuclear Mn III-Mn II -Mn III Complexes with a Tripodal Bridging Pyridylaminophenol Ligand. *New J. Chem.* **2016**, *40* (7), 6164–6170.
- (22) Bruker. *SAINT-Plus*, v.6.22; Bruker AXS Inc.: Madison, WI, USA, 2000.
- (23) Bruker. *SADABS*, v.2.05; Bruker AXS Inc.: Madison, USA, 2000.
- (24) Sheldrick, G. M. Crystal Structure Refinement with SHELXL. *Acta Crystallogr., Sect. C: Struct. Chem.* **2015**, *71* (1), 3–8.
- (25) Wrighton, M. S.; Ginley, D. S.; Morse, D. L. Technique for the Determination of Absolute Emission Quantum Yields of Powdered Samples. *J. Phys. Chem.* **1974**, *78* (22), 2229–2233.
- (26) do Nascimento Neto, J. A.; Valdo, A. K. S. M.; da Silva, C. C.; Guimarães, F. F.; Queiroz Júnior, L. H. K.; Maia, L. J. Q.; de Santana, R. C.; Martins, F. T. A Blue Light Emitting Cadmium Coordination Polymer with 75.4% External Quantum Efficiency. *J. Am. Chem. Soc.* **2019**, *141*, 3400.
- (27) Wyman, C.; Sloan, P.-P.; Shirley, P. Simple Analytic Approximations to the CIE XYZ Color Matching Functions. *J. Comput. Graph. Technol.* **2013**, *2* (2), 1–11.
- (28) McCamy, C. S. Correlated Color Temperature as an Explicit Function of Chromaticity Coordinates. *Color Res. Appl.* **1992**, *17* (2), 142–144.
- (29) Nolasco, M. M.; Vaz, P. M.; Vaz, P. D.; Ferreira, R. A. S.; Lima, P. P.; Carlos, L. D. A Green-Emitting  $\alpha$ -Substituted  $\beta$ -Diketonate Tb<sup>3+</sup> Phosphor for Ultraviolet LED-Based Solid-State Lighting. *J. Coord. Chem.* **2014**, *67* (23–24), 4076–4089.
- (30) Lannes, A.; Luneau, D. New Family of Lanthanide-Based Complexes with Different Scorpionate-Type Ligands: A Rare Case Where Dysprosium and Ytterbium Analogues Display Single-Ion-Magnet Behavior. *Inorg. Chem.* **2015**, *54* (14), 6736–6743.
- (31) Lapaev, D. V.; Nikiforov, V. G.; Safullin, G. M.; Lobkov, V. S.; Knyazev, A. A.; Krupin, A. S.; Galyametdinov, Y. G. UV Laser-Induced Enhancement of Photoluminescence Intensity in Vitrified Terbium(III)  $\beta$ -Diketonate Complex Film in Air. *J. Lumin.* **2018**, *194*, 407–413.
- (32) Ramesh, B.; Dillip, G. R.; Raju, B. D. P.; Somasundaram, K.; Peddi, S. P.; de Carvalho dos Anjos, V.; Joo, S. W. Facile One-Pot Synthesis of Hexagons of NaSrB<sub>5</sub>O<sub>9</sub>:Tb<sup>3+</sup> Phosphor for Solid-State Lighting. *Mater. Res. Express* **2017**, *4* (4), 046201.
- (33) Yang, X.-P.; Kang, B.-S.; Wong, W.-K.; Su, C.-Y.; Liu, H.-Q. Syntheses, Crystal Structures, and Luminescent Properties of Lanthanide Complexes with Tripodal Ligands Bearing Benzimidazole and Pyridine Groups. *Inorg. Chem.* **2003**, *42* (1), 169–179.
- (34) Akerboom, S.; Hazenberg, E. T.; Schrader, I.; Verbeek, S. F.; Mutikainen, I.; Fu, W. T.; Bouwman, E. O. -Oxazolonyl- and o-Thiazolonylphenol as Antennae in Luminescent Eu(III) and Tb(III) Complexes. *Eur. J. Inorg. Chem.* **2014**, *2014* (28), 4896–4906.
- (35) Dieke, G. H. *Spectra and Energy Levels of Rare Earth Ions in Crystals*; Wiley-Interscience: New York, USA, 1968.
- (36) Linganna, K.; Ju, S.; Basavapoornima, C.; Venkatramu, V.; Jayasankar, C. K. Luminescence and Decay Characteristics of Tb<sup>3+</sup>-Doped Fluorophosphate Glasses. *J. Asian Ceram. Soc.* **2018**, *6* (1), 82–87.
- (37) Linganna, K.; Sreedhar, V. B.; Jayasankar, C. K. Luminescence Properties of Tb<sup>3+</sup> Ions in Zinc Fluorophosphate Glasses for Green Laser Applications. *Mater. Res. Bull.* **2015**, *67*, 196–200.
- (38) Gálico, D. A.; Souza, E. R.; Mazali, I. O.; Sigoli, F. A. High Relative Thermal Sensitivity of Luminescent Molecular Thermometer Based on Dinuclear [Eu<sub>2</sub>(Mba)<sub>4</sub>( $\mu$ -Mba)<sub>2</sub>(H<sub>2</sub>O)<sub>2</sub>] Complex: The Role of Inefficient Intersystem Crossing and LMCT. *J. Lumin.* **2019**, *210*, 397–403.
- (39) Lapaev, D. V.; Nikiforov, V. G.; Lobkov, V. S.; Knyazev, A. A.; Galyametdinov, Y. G. A Photostable Vitrified Film Based on a Terbium(III)  $\beta$ -Diketonate Complex as a Sensing Element for Reusable Luminescent Thermometers. *J. Mater. Chem. C* **2018**, *6* (35), 9475–9481.
- (40) Chen, X.-Y.; Marchal, C.; Filinchuk, Y.; Imbert, D.; Mazzanti, M. A Flexible Tripodal Ligand Linking Octametallate Terbium Rings into Luminescent Polymeric Chains. *Chem. Commun.* **2008**, No. 29, 3378.
- (41) Song, X.-Q.; Dong, W.-K.; Zhang, Y.-J.; Liu, W.-S. Synthesis and Luminescence Properties of Lanthanide Complexes with a New Tripodal Ligands Featuring Salicylamide Arms. *Luminescence* **2010**, *25* (4), 328–335.
- (42) Murase, M.; Yamauchi, S.; Sakamoto, S.; Takahashi, S.; Matsumoto, N.; Tsuchimoto, M. Enantioselective Aggregation and Luminescence Properties of Europium(III) and Terbium(III) Complexes of an Acetate and a Tripodal Ligand Containing Three Imidazole Groups. *Polyhedron* **2013**, *59*, 76–84.
- (43) Hansch, C.; Leo, A.; Taft, R. W. A Survey of Hammett Substituent Constants and Resonance and Field Parameters. *Chem. Rev.* **1991**, *91* (2), 165–195.
- (44) Latva, M.; Takalo, H.; Mukkala, V.-M.; Matachescu, C.; Rodríguez-Ubis, J. C.; Kankare, J. Correlation between the Lowest

Triplet State Energy Level of the Ligand and Lanthanide(III) Luminescence Quantum Yield. *J. Lumin.* **1997**, *75* (2), 149–169.

(45) Li, H. L.; Wang, Z. L.; Xu, S. J.; Hao, J. H. Improved Performance of Spherical BaWO<sub>4</sub>:Tb<sup>3+</sup> Phosphors for Field-Emission Displays. *J. Electrochem. Soc.* **2009**, *156* (5), J112.